This is a repository copy of *Comparison of in vivo lung morphometry models from 3D multiple b-value 3He and 129Xe diffusion-weighted MRI*.

White Rose Research Online URL for this paper:
https://eprints.whiterose.ac.uk/138384/

Version: Accepted Version

Comparison of in vivo lung morphometry models from 3D multiple b-value ^{3}He and ^{129}Xe diffusion-weighted MRI

Ho-Fung Chan[1], Guilhem J. Collier[1], Nicholas D. Weatherley[1,2], Jim M. Wild[1,3]

[1]POLARIS, Academic Unit of Radiology, Infection, Immunity & Cardiovascular Disease, University of Sheffield, Sheffield, UK

[2] Academic Directorate of Respiratory Medicine, Sheffield Teaching Hospitals NHS Foundation Trust, Sheffield, UK

[3] Insigneo, Institute for in silico medicine, University of Sheffield, Sheffield, UK

Corresponding Author: Jim M. Wild

Email: j.m.wild@sheffield.ac.uk

Address: Academic Unit of Radiology, University of Sheffield, C Floor, Royal Hallamshire Hospital,

Glossop Road, Sheffield, S10 2JF, UK

Phone Number: + 44 (0)114 2159141

Word Count: 4925

Running title: Comparison of ^{3}He and ^{129}Xe DW-MRI lung morphometry models

Abstract

Purpose: To compare in vivo lung morphometry parameters derived from theoretical gas diffusion models, the cylinder model (CM) and stretched exponential model (SEM), in a range of acinar microstructural length scales encountered in healthy and diseased lungs with ^{3}He and ^{129}Xe diffusion-weighted (DW) MRI.

Methods: 3D multiple b-value ^{3}He and ^{129}Xe DW-MRI was acquired with compressed sensing at 1.5 T from 51 and 31 subjects, respectively that included: healthy volunteers, ex-smokers, idiopathic pulmonary fibrosis, and chronic obstructive pulmonary disease patients. For each subject, the SEM-derived mean diffusive length scale (Lm_D) was calculated from the diffusion signal decay, and was compared to the CM-derived mean chord length (Lm) and mean alveolar diameter (L_{Alv}) in order to determine the relationships between the different lung morphometry parameters.

Results: For both ^{3}He and ^{129}Xe DW-MRI, the mean global Lm_D value was significantly related ($P<0.001$) to Lm in a non-linear power relationship; while the L_{Alv} demonstrated excellent linear correlation ($P<0.001$) with Lm_D. A mean bias of +1.0% and -2.6% towards Lm_D was obtained for Bland-Altman analyses of ^{3}He and ^{129}Xe Lm_D and L_{Alv} values, suggesting the two morphometric parameters are equivalent measures of mean acinar dimensions.

Conclusion: Within the experimental range of parameters considered here for both ^{3}He and ^{129}Xe, the SEM-derived Lm_D is related non-linearly to CM-derived Lm, and demonstrates excellent agreement with the CM-derived L_{Alv}.

Keywords: lung morphometry, cylinder model, stretched exponential model, hyperpolarized ^{129}Xe, hyperpolarized ^{3}He

Introduction

Inhaled hyperpolarized noble gases [3]He and [129]Xe are sensitive to underlying changes in the alveolar microstructure through the measurement of the apparent diffusion coefficient (ADC) with diffusion-weighted MRI (DW-MRI) [1, 2]. The diffusion regime of hyperpolarized gases in the lungs is however non-Gaussian, resulting in non-mono-exponential signal attenuation with increasing b-value [3]. This non-Gaussian phase dispersion has a significant bearing on the derivation of quantitative information about lung microstructure from in vivo DW-MRI, and as such there is no direct one-to-one quantitative correspondence between the measured ADC value and histological parameters of lung morphometry. Theoretical models of gas diffusion have been proposed to account for the non-Gaussian diffusion signal behaviour and derive estimates of lung alveolar length scales from the multiple b-value hyperpolarized gas diffusion MR signal.

Much work has been performed in modelling the effects of restricted diffusion inside geometrical models of lung microstructure that include: cylindrical geometries [4-6], acinar trees [7], branching structures [8-10], alveolar ducts [11], and porous media models [12, 13]. Alternative strategies have also been proposed that do not rely upon geometrical assumptions of acinar structure such as q-space transform analysis [14, 15], diffusion kurtosis [16] and stretch exponential mathematical models [17-19]. The cylinder model (CM) [4-6], and the stretched exponential model (SEM) [17-19] are two theoretical gas diffusion models that can derive in vivo measurements of acinar length scale on a voxel-by-voxel basis. These two gas diffusion models have been used, with both [3]He and [129]Xe, to study changes in lung microstructure associated with smoking-related early emphysema [19-21], chronic obstructive pulmonary disease (COPD) [19, 22, 23], asthma [17], age [24], lung inflation [25], lung growth [26], and paediatric lung transplant lifespan [27].

Currently, the relationship between the estimates of alveolar dimension from these two models is relatively unknown. Estimates of mean chord length (Lm) from the CM, and mean diffusive length scale (Lm_D) from the SEM were compared recently in older never smokers, ex-smokers, and COPD patients with [3]He multiple b-value DW-MRI at 3 T [23]. A linear correlation between Lm and Lm_D was obtained suggesting the lung morphometry parameters are related but not equivalent. However, in this analysis the SEM-derived Lm_D was implemented in a simplified form to that in the original study [17], potentially affecting the observed linear correlation seen there (see Discussion).

This work compares the SEM and CM in vivo at 1.5 T with 3D multiple b-value [3]He and [129]Xe DW-MRI acquired in a range of patient groups representing different acinar length scales. The two theoretical gas diffusion models, SEM and CM, were used to evaluate each dataset and derive in vivo lung morphometry parameters. For each [3]He and [129]Xe dataset, the CM-derived mean chord length (Lm), and mean alveolar diameter (L_{Alv}) were compared to the SEM-derived mean diffusive length scale (Lm_D).

Theory

Cylinder model

In the cylinder model (CM), the acinar airway is modelled as infinitely long cylinders covered by alveoli according to Haefeli-Bleuer and Weibel [28]. Assuming a uniform distribution of cylinders in all orientations within a measured voxel, the total signal attenuation, for given diffusion-weighted b-values, can be described as a superposition of mono-exponential signals from each individual airway [6]:

$$\frac{S(b)}{S_0} = \exp(-bD_T)\left(\frac{\pi}{4bD_{AN}}\right)^{1/2} \cdot \Phi[(bD_{AN})^{1/2}] \tag{1}$$

where D_L and D_T are longitudinal and transverse diffusion coefficients, $D_{AN} = D_L - D_T$, and Φ is the error function. The CM geometry implemented in this work was based upon an eight alveolus model [29], where the effective alveolar diameter (L_{Alv}) is equivalent along the airway and across the alveolus, and is 1/8 of the chord length of the cylindrical acinar airway (Figure 1):

$$L_{Alv} = 2R\sin(\pi/8) = 0.765R \tag{2}$$

Figure 1 – here

The CM is characterized by two geometrical parameters, the outer acinar airway radii (R) and alveolar sleeve depth (h), that are related to D_L and D_T by the following phenomenological expressions [29]:

$$D_L = D_{L0}(1 - \beta_L \cdot bD_{L0}); \quad D_T = D_{T0}(1 + \beta_T \cdot bD_{T0}) \tag{3}$$

$$\frac{D_{L0}}{D_0} = \exp[-2.89 \cdot (h/R)^{1.78}]; \quad \beta_L = 35.6 \cdot (R/\ell_1)^{1.5} \cdot \exp\left[-4/\sqrt{h/R}\right] \tag{4}$$

$$\frac{D_{T0}}{D_0} = \exp[-0.73 \cdot (\ell_2/R)^{1.4}] \cdot [1 + \exp(-A \cdot (h/R)^2 \cdot u(h/R))]$$

$$u(h/R) = \exp(-5 \cdot (h/R)^2) + 5 \cdot (h/R)^2 - 1 \tag{5}$$

$$A = 1.3 + 0.25 \cdot \exp(14 \cdot (R/\ell_2)^2)$$

where $\ell_1 = \sqrt{2\Delta D_0}$ and $\ell_2 = \sqrt{2}\ell_1$ are the respective 1D and 2D characteristic free diffusion lengths of ³He diluted in air. Within the prescribed physiological range of the CM ($h/R < 0.6$), the β_T parameter is constant at 0.06 [29]. The above expressions are valid, within an estimation accuracy of ~1-3%, for R = 300 - 400 µm, and diffusion times (Δ) of 1.5 to 2 ms [29, 30]; therefore, incorporating alveolar parameters ranging from healthy to mild emphysema. After the estimation of R and h, additional parameters such as the alveolar volume (V_{Alv}) and alveolar surface area (S_{Alv}) can be derived based upon the cylindrical airway geometry (Figure 1):

$$V_{Alv} = \frac{\pi}{8}R^2 L_{Alv}; \quad S_{Alv} = \frac{\pi}{4}R \cdot L_{Alv} + \frac{\pi}{4}h \cdot (2R - h) + 2h \cdot L_{Alv} \tag{6}$$

The alveolar volume includes both the volume of the alveolar duct and the alveolus. With S_{Alv} and V_{Alv}, the mean chord length (Lm) can be estimated using the histological relationship between Lm and surface-to-volume ratio [31]. In the calculation of Lm, the thickness of the alveolar wall (~10 µm), is neglected such that the mean chord length is equivalent to the mean linear intercept.

$$Lm = \frac{4V_{Alv}}{S_{Alv}} \qquad (7)$$

Due to the inherent differences in diffusivity (D_0) and gyromagnetic ratio (γ) of [3]He and [129]Xe, the [3]He CM phenomenological expressions cannot be directly applied for [129]Xe DW-MRI. In Sukstanskii et al. [5], new phenomenological expressions were derived for [129]Xe DW-MRI at $\Delta = 5$ ms; however, it was also noted that when the same theoretical free diffusion length is probed with both nuclei (i.e. $\Delta_{He} = 1.6$ ms and $\Delta_{Xe} = 10$ ms), the original [3]He-based expressions should in theory be valid. However, in our recent work with the derivation of an empirically-optimized [129]Xe $\Delta = 8.5$ ms [19], it was concluded that comparable [3]He and [129]Xe CM Lm can be obtained at this diffusion time using the [3]He-based CM phenomenological expressions. Therefore, in this work where a [129]Xe $\Delta = 8.5$ ms is implemented, [129]Xe-derived R and h were related to [129]Xe D_L and D_T coefficients using the same expressions as for the [3]He data (Equations 3-5).

Stretched exponential model

An alternative theoretical model for describing the hyperpolarized gas diffusion signal behaviour in the lungs is the stretched exponential model (SEM) [17]. The SEM describes intra-voxel non-mono-exponential signal behaviour without an assumption on the number of contributing sources and their respective distributions. Previous applications of the SEM include proton DW-MRI experiments in the brain and prostate, which demonstrated a better characterization of the heterogeneous intra-voxel diffusion rates than mono- and bi-exponential diffusion models [32, 33].

The SEM is a plausible candidate for modelling gas diffusion signal behaviour in the lungs where within each [3]He or [129]Xe imaging voxel, the diffusion of gas atoms is restricted by the walls of airways with different sizes and orientations with respect to the 1D diffusion-sensitizing gradient leading to different local diffusion regimes and apparent diffusion rates. Hence, the measured macroscopic voxel signal can be represented as the superposition of signals with different apparent diffusivities (D):

$$\frac{S(b)}{S_0} = \int_0^{D_0} p(D)e^{-bD}dD \qquad (8)$$

where S_0 is the signal when b = 0, $S(b)$ is the signal corresponding to a non-zero b-value, D_0 is the respective free diffusion coefficient of [3]He or [129]Xe diluted in air or N_2, and $p(D)$ is the probability distribution of different apparent diffusivities. A numerical expression of $p(D)$ can be obtained for the non-mono-exponential signal decay by using a stretched exponential function, that accounts for the

4

non-Gaussian nature of the diffusion MR signal [34]. The stretched exponential function is defined as follows:

$$\frac{S(b)}{S_0} = e^{[-b \cdot DDC]^{\alpha}} \tag{9}$$

where *DDC* is the distributed diffusivity coefficient, and α is the heterogeneity index that describes the deviation from a mono-exponential decay (corresponding to α = 1). The $p(D)$ distribution is interpreted as the underlying heterogeneity of the observed diffusion signal decay, within a voxel, introduced either by underlying structural heterogeneity or changes in localized diffusion regime, and can be estimated from stretched exponential function parameters using [35]:

$$p(D) = \tau_0 \frac{B}{D\tau_0^{(1-\alpha/2)/(1-\alpha)}} \cdot \exp\left[-\frac{(1-\alpha)\alpha^{\alpha/(1-\alpha)}}{D\tau_0^{\alpha/(1-\alpha)}}\right] \cdot f(D) \tag{10}$$

where τ_0 is 1/DDC, and $f(D)$ is defined by:

$$f(D) = \begin{cases} 1/[1 + C(D\tau_0)^{\delta}], & \delta = \alpha\,(0.5 - \alpha)/(1 - \alpha), \ \alpha \leq 0.5, \\ 1 + C(D\tau_0)^{\delta}, & \delta = \alpha\,(\alpha - 0.5)/(1 - \alpha), \ \alpha > 0.5, \end{cases} \tag{11}$$

The parameters *B* and *C* are functions of α, and values of these parameters for specific α values are tabulated in Table 1 of Berberan-Santos et al. [35]. For other α values, corresponding *B* and *C* parameters are derived through interpolation. The expression for $p(D)$ can subsequently be related to a probability distribution of diffusion length scales $p(L_D)$ associated with the different apparent diffusivities (*D*) with the 1D characteristic diffusion length equation (i.e. root mean squared displacements):

$$L_D = \sqrt{2\Delta D} \tag{12}$$

where Δ is the diffusion time. The $p(L_D)$ distributions represent a measure of the distribution of microscopic dimensions of the airways, such as the different diffusion-restricting boundaries, contained within a given voxel. From the $p(L_D)$ distribution, the expectation value or mean diffusive length scale (*Lm_D*) can be derived for each voxel from:

$$Lm_D = \int_0^{D_0} \sqrt{2\Delta D}\, p(D)\, dD = \int_0^{\ell_1} p(L_D)\, dL_D \tag{13}$$

where $\ell_1 = \sqrt{2\Delta D_0}$ is the 1D characteristic free diffusion length. In summary, we hypothesize that *Lm_D* values from the SEM can provide quantitative estimates of the mean acinar airway dimensions within a voxel without a geometrical assumption of the underlying lung microstructure.

Methods

In this retrospective analysis with UK National Research Ethics Committee approval, 3D multiple b-value ^{3}He and ^{129}Xe DW-MRI was acquired in 51 and 31 subjects, respectively, representing a range of acinar length scales from different pulmonary patient groups including: healthy volunteers, ex-smokers, idiopathic pulmonary fibrosis (IPF), and COPD patients. Within this cohort of subjects, a subgroup of 13 subjects had both ^{3}He and ^{129}Xe data acquired.

^{3}He and ^{129}Xe DW-MRI was both acquired on a 1.5 T GE HDx scanner using flexible quadrature transmit/receive vest coils (Clinical MR Solutions, Brookfield, Wisconsin, USA) following the inhalation of a 1L gas mixture from functional residual capacity (FRC) with 3D spoiled gradient echo sequences and compressed sensing (CS) [18, 19]. 3D ^{3}He DW-MRI acquisition parameters were: 250 ml hyperpolarized ^{3}He (~25% polarization) (balanced with 750 ml of N_2), 4 interleaves (b = 0, 1.6, 4.2, 7.2 s/cm^2), field of view = 40x32.5x28.8 cm^3, voxel size = 4.17x4.17x12 mm^3, TE/TR = 4.2/6.0 ms, diffusion time = 1.6 ms (maximum diffusion gradient strength = 30 mT/m, ramp = 0.3 ms, plateau = 1.0 ms), flip angle = 1.9°, and bandwidth = ±31.25 kHz. 3D ^{129}Xe DW-MRI acquisition parameters were: 550 ml hyperpolarized ^{129}Xe (~30% polarization [36]) (balanced with 450 ml of N_2), 4 interleaves (b = 0, 12, 20, 30 s/cm^2), field of view = 40x32.5x27 cm^3, voxel size = 6.25x6.25x15 mm^3, TE/TR = 14.0/17.3 ms, diffusion time = 8.5 ms (maximum diffusion gradient strength = 32.6 mT/m, ramp = 0.3 ms, plateau = 2.3 ms, gap = 5.6 ms), flip angle = 3.1°, and bandwidth = ±6.97 kHz. The respective diffusion times chosen for the two gases (Δ_{He} = 1.6 ms, and Δ_{Xe} = 8.5 ms) were empirically optimized such that comparable mean Lm_D and Lm measurements are obtained with both ^{3}He and ^{129}Xe [19].

All CS reconstructions and lung morphometry calculations were implemented in-house using MATLAB (MathWorks, Natick, Massachusetts, USA) software. Each CS under-sampled dataset was reconstructed with previously optimized parameters that were scaled by the relative difference between total intensity of the k-space data within the acquired CS under-sampled dataset and the optimal retrospectively CS under-sampled dataset [18, 19]. Lung regions were manually segmented from the reconstructed diffusion-weighted MR images, and ^{3}He and ^{129}Xe DW-MRI metrics of lung microstructure were calculated for each imaging voxel. ADC values were estimated from a two b-value fit (b = 0 and 1.6 s/cm^2 for ^{3}He, and b = 0 and 12 s/cm^2 for ^{129}Xe), and SEM and CM metrics (see Theory section) were derived from the multiple b-value fit to the two theoretical gas diffusion models. For the SEM, voxels were retained that returned a DDC value between 0 and the D_0 of the respective gas, and an alpha value between 0 and 1. While for the CM, a voxel is retained when a R<700 µm and r<600 µm values is returned from the model.

One-way analysis of variance (ANOVA) with Tukey post-hoc multiple comparison adjustment was conducted to compare lung morphometry metrics across the different patient groups. Pearson's correlation coefficients, and regression model curve fits were used to quantify the relationship between

the diffusion model lung morphometry parameters. All statistical analyses were performed using IBM SPSS Statistics (Version 23.0, Armonk, NY) and GraphPad Prism (San Diego, USA), and statistical significance level was set at $P<0.05$.

Results

^{3}He lung morphometry comparison

Maps of lung morphometry parameters were generated for each ^{3}He dataset, and a summary of mean ^{3}He DW-MRI metrics for each subject group is provided in Table 1. The SEM successfully fitted all ^{3}He voxels for all subject groups. However, for the accepted range specified for the CM (see Methods), the CM returned fewer voxels in the maps from the lungs of the IPF and COPD subject groups, with an average of 94.5% ± 8.2%, and 71.5% ± 24.4% of voxels successfully fitted, respectively (Table 1). A statistically significant ($P<0.001$) difference in mean global value across the patient groups was obtained via ANOVA for each ^{3}He DW-MRI metric. A significant increase ($P<0.05$) in mean ADC, DDC, Lm_D, R, L_{Alv}, and Lm, and a significant decrease ($P<0.05$) in mean α and h, was observed between the following patient groups: healthy and IPF; healthy and COPD; ex-smoker and IPF; ex-smoker and COPD; and IPF and COPD. In contrast, no significant difference was observed between healthy volunteers and ex-smoker patients for all lung morphometry parameters. Example maps of ^{3}He lung morphometry indices from the SEM and CM (Figure 2) illustrate this difference in lung microstructure between subject groups.

A statistically significant correlation ($P<0.001$) between global mean ^{3}He Lm_D and Lm was observed. Three different curve regression fits (linear, exponential, and power) were performed, and all three fits had similar R^2 values (Table 2). For each regression fit, Lm was the dependent variable (β_0), and Lm_D was set as the independent variable (β_1). The power regression fit had the largest R^2 (0.960) and is presented in Figure 3a. A statistically significant correlation ($P<0.001$) between Lm_D and L_{Alv} parameters was also obtained. A linear regression fit with Lm_D and L_{Alv} as independent (β_1) and dependent (β_0) variables, respectively, derived a linear slope (β_1) of 1.00, suggesting excellent agreement between the two parameters (Figure 3b). Bland-Altman analysis confirmed this agreement with a mean bias in Lm_D value of +1.0% and 95% of the difference was between -3.2% to 5.1% (Figure 4a).

^{129}Xe lung morphometry comparison

The equivalent mean ^{129}Xe lung morphometry parameters for each subject group are summarized in Table 1. For all subject groups, the SEM successfully fitted all ^{129}Xe voxels; while for the ^{129}Xe CM, a similar trend in fewer voxels successfully returned was observed for the IPF ($99.6\% \pm 0.8\%$) and COPD ($94.2\% \pm 11.5\%$) subject groups (Table 1). Similar to the ^{3}He lung morphometry parameters, all ^{129}Xe metrics (except for α value) were significantly different ($P<0.001$, via ANOVA), across the subject groups. A significant increase ($P<0.05$) in mean ^{129}Xe ADC, DDC, Lm_D, R, L_{Alv}, and Lm, alongside a significant decrease ($P<0.05$) in mean ^{129}Xe h, was observed between healthy and IPF, healthy and COPD, and ex-smoker and COPD patient groups only. No significant difference was observed between the other patient groups for all lung morphometry parameters. Examples of ^{129}Xe lung morphometry maps from the SEM and CM for each subject group are shown in Figure 5.

A statistically significant correlation ($P<0.001$) between ^{129}Xe Lm_D and Lm was obtained. The same three curve regression fits (linear, exponential, and power) were performed, and as for ^{3}He, all three fit curves had similar R^2 values (Table 2). ^{129}Xe Lm_D and Lm can be described by a power regression fit with $R^2 = 0.971$ that is presented in Figure 3c. The ^{129}Xe parameters Lm_D and L_{Alv} were also significantly correlated ($P<0.001$) in a linear relationship (Figure 3d), and the linear slope fit (β_1) of 1.05 suggests excellent agreement. This was confirmed with Bland-Altman analysis, and a mean bias in Lm_D value of -2.6% and 95% of the difference was between -7.9% to 2.7% (Figure 4b).

<u>Figure 5 – here</u>

Discussion

Comparison of Lm_D with Lm and L_{Alv}

In this in vivo comparison of ^{3}He and ^{129}Xe theoretical gas diffusion lung morphometry models, significant differences ($P<0.001$) between subject groups were observed. Lung morphometry parameters were significantly increased (ADC, DDC, Lm_D, R, L_{Alv}, and Lm) or decreased (α and h) ($P<0.05$) between healthy subjects and COPD patients. These significant differences reflect enlarged acinar airspaces associated with emphysematous destruction and loss of alveolar elasticity in COPD [19, 22, 23]. To our knowledge, in vivo DW-MRI metrics from lungs of patients with IPF have not been reported before. Lung morphometry parameters for IPF patients, from both the SEM and CM, were significantly different ($P<0.05$) to healthy subjects, and appear to lie between the ranges of metrics from the ex-smokers and COPD patient groups. This is presumed to be related to the honeycomb changes observed in cross-sectional imaging and the microscopic bronchiolization process in the distal airways.

While no significant differences in lung morphometry parameters was obtained between healthy and ex-smoker volunteers, a trend towards more severe microstructural metrics was observed that matches the results observed with ADC [37, 38] and lung morphometry parameters [19-21] in previous studies.

Mean [3]He CM-derived parameters of R, h and Lm (Table 1) were comparable to the values reported in the literature for healthy ($R = 304$ µm, $h = 154$ µm, $Lm = 186$ µm) [24], ex-smokers ($R = 304$, $h = 130$, $Lm = 220$) [21], and COPD patients ($R = 450$, $Lm = 450$) [23]. Mean [3]He SEM metrics for healthy and COPD subjects also matched previously reported DDC (healthy = 0.14 cm^2/s, COPD = 0.39 cm^2/s), α (healthy = 0.86, COPD = 0.69), and Lm_D (healthy = 210 µm, COPD = 293 µm) values [18, 39]. Ex-smoker SEM metrics were also comparable to reported values (DDC = 0.21 cm^2/s, $\alpha = 0.81$) [23]. The [129]Xe α value was the same for all groups, and was larger than the equivalent [3]He α value. This could be attributed to the more mono-exponential signal decay (i.e. larger α values) observed with [129]Xe when compared to [3]He DW-MRI.

The regression model parameters for each regression curve fit (Table 2) were similar for both [3]He and [129]Xe. This indicates comparable correlations between morphometry parameters are observed with both gases, and slight differences in regression model parameters can be associated with the inherent differences in the [3]He and [129]Xe subject groups. The R^2 values for the three different regression curve fits of the [3]He and [129]Xe comparison of Lm and Lm_D were almost identical. The linear regression fit R^2 (0.956) was very similar to the power regression model (0.960); however, a power relationship matched the [3]He and [129]Xe data best. To date, the only previous comparison between the CM and SEM gas diffusion models was performed at 3 T with 2D [3]He multiple b-value DW-MRI [23]. In this previous comparison, a statistically significant linear trend was observed between [3]He Lm_D and Lm parameters (Figure 6).

Figure 6 – here

The first possible contributing factor to this observed difference in lung morphometry parameter relationships is the discrepancy in the derivation of Lm_D between the two studies. In Ouriadov et al. [23], Lm_D was calculated, using the 1D theoretical diffusion length equation, from a mean diffusivity value ($\overline{D}$) obtained from the probability distribution of diffusivities $p(D)$ given by:

$$\overline{D} = \int_0^{D_0} p(D) \, dD$$

(14)

$$Lm_D = \sqrt{2\Delta\overline{D}}$$

While in our comparison, Lm_D is defined as the expectation value of a probability distribution of length scales, $p(L_D)$, obtained by transforming $p(D)$ using the 1D theoretical diffusion length equation. This non-linear transformation of the 1D theoretical diffusion length equation is applied within the continuous integral (Equation 13). In contrast, the application of the non-linear transformation on the

expected diffusivity or mean diffusivity ($\overline{D}$) in order to derive Lm_D in Equation 14 is not generally equivalent to the Lm_D derived in this comparison (see Equation 15).

$$\int\limits_{0}^{D_0} \sqrt{2\Delta D}\; p(D)\; dD \;\neq\; \sqrt{2\Delta \int\limits_{0}^{D_0} p(D)\; dD} \tag{15}$$

A second possible factor is differences in subject cohorts; for example, the healthy cohort in the 3 T comparison of Ouriadov et al. [23] were older never-smokers (mean age = 69), while the cohort in this comparison at 1.5 T were considerably younger (mean age = 26). In Figure 6, the inclusion of young healthy volunteers with expected smaller alveolar dimensions contributes significantly to the non-linear power relationship observed at 1.5 T. If our healthy subject data are excluded, a linear correlation with a slope gradient of 5.0 is obtained that is similar to the one observed at 3 T (gradient = 4.3). The last factor that could contribute to the different lung morphometry relationships is the difference in magnetic field strength of the respective measurements made in the two studies. Susceptibility gradients are induced at the tissue and air interfaces within the acinar space, and these background field gradients are field strength dependent and have been shown to affect ADC and theoretical gas diffusion model parameters with [3]He at 1.5 T when compared to 3 T [40]. Measurements of CM-derived Lm at 3 T in healthy volunteers were up to 17% larger than the equivalent measurements at 1.5 T [40], and this could in part explain the larger [3]He Lm values observed at 3 T.

The power relationship observed between Lm and Lm_D, suggests that even though the two lung morphometry parameters are significantly related, they are not totally equivalent measures of alveolar dimension. The linear correlation and regression parameters between Lm_D and L_{Alv} for both [3]He and [129]Xe indicates excellent agreement between the two lung morphometry parameters. Bland-Altman comparison of mean Lm_D and L_{Alv} values (Figure 4) confirmed this excellent agreement with a mean bias of 1.0% and -2.6% obtained for [3]He and [129]Xe, respectively.

SEM and CM differences and limitations

The in vivo results suggest that mean diffusive length scale (Lm_D) from the SEM is more analogous to the mean alveolar diameter (L_{Alv}) than the mean chord length (Lm) from the CM. Due to the differences in how each parameter is calculated, the portion of the acinar airway geometry that is represented by each parameter is slightly different, and this may go towards explaining the two distinct relationships of Lm_D between Lm and L_{Alv}. In the SEM, where no assumptions of acinar airway geometry are made, Lm_D is directly reflective of the apparent distance [3]He or [129]Xe gas atoms can diffuse within the acinar airspace. The maximum Lm_D is therefore limited by the theoretical free diffusion length of the DW-MRI experiments (~500 µm), which is dependent upon the experimental diffusion time and respective free diffusion coefficient of the gas. According to histological measurements of the pulmonary acinus, the mean alveolar diameter in healthy adult lungs is approximately 200 to 250 µm [31, 41, 42], and the

mean alveolar duct diameter ranges from 200 to 600 µm [31]. Therefore, as the majority of lung volume consists of the alveolar airspace, gas atoms in these experiments are predominantly restricted by the alveolar geometry and as such Lm_D is interpreted as being reflective of alveolar dimensions.

In contrast, the CM-derived mean chord length (Lm) is calculated through an inferred relationship between the volume and surface area of a single alveolus unit (Equation 7). It is important to note that the histological Lm is not solely a measurement of alveolar size, but rather a measurement of the acinar airspace that includes the alveolus and alveolar ducts [43]. This is apparent in the calculation of V_{Alv} (Equation 6) in the cylinder model, which includes both alveolus and alveolar duct volumes. The inclusion of the alveolar duct volume could in theory allow the calculation of Lm values that exceed the theoretical free diffusion length of the gas alone.

This could explain why in predominantly healthy subjects where the gas atoms can diffuse out of the alveoli and into the alveolar duct, there is a reasonable matching of Lm_D and Lm values. However, in patients with more advanced disease where alveolar walls are destroyed, the gas atoms diffuse more freely between enlarged alveoli and alveolar ducts. While a Lm measurement can still be derived, it may exceed the theoretical free diffusion length (see data points above dotted line in Figure 6). These conditions can cause a large mismatch in Lm_D and Lm values when large microstructural changes occur, and is demonstrated in the respective maps from the lungs of a representative IPF and COPD patient in Figure 2 and 5. With increasingly advanced disease the mean Lm_D value will plateau towards the theoretical free diffusion length, while the Lm value will theoretically continue to increase, and this accounts for the power relationship obtained in this in vivo comparison.

The L_{Alv} values demonstrated excellent agreement with Lm_D values with both [3]He and [129]Xe, indicating that the two parameters may be analogous measurements of alveolar dimensions. This quantitative matching stems from the underlying CM geometry, where the cylinder duct is surrounded by an alveolar sleeve consisting of eight alveolus units [29]. The number of alveoli was chosen such that the chord length or diameter of an alveolus unit (L_{Alv}) would empirically match the alveolar diameter obtained from histological measurements. Previous studies of in vivo lung morphometry with the CM did not report L_{Alv} values, but L_{Alv} can be retrospectively calculated from the published acinar airway radii (R) values ($L_{Alv} = 0.765R$). The retrospectively calculated [3]He L_{Alv} in healthy (~230 µm [24]), ex-smokers (~250 µm [21]), and COPD (~340 µm [23]) patients are similar to those for [3]He and [129]Xe derived in this in vivo comparison (healthy ~210 µm; ex-smoker ~230 µm; COPD ~300 µm).

The CM has a specific prescribed physiological range of operation, such as $h/R < 0.6$ and $R = 300$ to 400 µm, where the phenomenological expressions relating the anisotropic diffusion coefficients and alveolar duct dimensions are considered valid within an estimation accuracy of ~1-3% [29, 30]. In this work, an upper limit of $R = 700$ µm and $r = 600$ µm was prescribed during the fitting of the multiple b-value diffusion signal, and DW-MRI voxels that exceed these limits were excluded from the CM

morphometry maps, representing regions where alveolar duct dimensions far exceed the specified range for the CM. Within the theoretical boundaries of the CM, anisotropic diffusion in a cylindrical acinar airway geometry can be assumed. However, in lungs with significant destruction of the alveolar walls due to advanced lung disease, the diffusion in the enlarged acinar airspace is more isotropic and can no longer be described by anisotropic restricted diffusion. It is also important to note that in the CM, the mean chord length (Lm) is assumed to be equivalent to the mean linear intercept length due to the assumption of a negligible alveolar wall thickness [29]. However, this assumption may not be valid in diseases such as IPF where interstitial wall thickening is an established feature of the microstructural pathology.

Figure 7 – here

These 'missing' voxels contribute to the smaller percentage of successfully fitted CM voxels observed predominantly for IPF and COPD subject groups in Table 1, and are demonstrated for representative L_{Alv} maps from three COPD patients in Figure 7. The regions of 'missing' voxels in the COPD L_{Alv} maps are not associated with unventilated lung regions, and the corresponding regions exist in the Lm_D maps because the SEM returns a fit of the diffusion signal in voxels containing advanced emphysema or those corresponding to conducting airways that show free and/or localized diffusion behaviour. This limitation of the CM suggests that the two theoretical gas diffusion models may have different operational ranges of length scale estimation accuracy, perhaps due to inherent differences in their geometrical and mathematical assumptions.

Even though the SEM appears to derive estimates of diffusive length scale across all ranges of acinar structural length scales (up to the theoretical free diffusion length), we emphasize that it has not yet been directly validated against histology or in phantoms with known geometries, and a firm theoretical basis of microstructural estimates awaits. In particular, the expression in Equation 10 is taken directly from Berberan-Santos et al. [35], and there is not yet a complete physical explanation of how this distribution function translates to a distribution of diffusion length scales in the lungs and its underlying structural heterogeneity. Validating the Lm_D values with histology would increase the clinical potential of this diffusion model in the longitudinal monitoring of lung microstructural changes with hyperpolarized gas DW-MRI. Currently, Lm_D results are either qualitatively compared to lung morphometry measurements derived from histology in similar subject populations or validated against CM-derived measurements from the same diffusion data. However, the results in [19] demonstrate that the SEM-derived Lm_D is dependent upon experimental diffusion time. Therefore, it is possible that the [3]He, and subsequently the [129]Xe, diffusion time will need to be tuned such that derived Lm_D results match those in the validation geometry. In future work, finite element simulations of gas diffusion signal behaviour in known geometries [44, 45] will be used to further explore the relationship between the two

diffusion models, validate the lung morphometry parameters derived from them, and to gain further theoretical insight into each models' physical meaning and range of applicability.

Conclusions

This work presents the first in vivo comparison of the stretched exponential model (SEM) and cylinder model (CM) lung morphometry parameters with both ^{3}He and ^{129}Xe DW-MRI at 1.5 T. The morphometry parameters from the two diffusion models are significantly related where CM-derived mean chord length (Lm) and SEM-derived mean diffusive length scale (Lm_D) are correlated in a non-linear power relationship; while Lm_D and CM-derived mean alveolar diameter (L_{Alv}) demonstrate excellent linear agreement. The two distinct relationships are thought to be representative of the different parts of the acinar airway geometry that are measured with each lung morphometry parameter.

Acknowledgements

[1]   B. T. Saam, D. A. Yablonskiy, V. D. Kodibagkar, J. C. Leawoods, D. S. Gierada, J. D. Cooper*, et al.*, "MR imaging of diffusion of 3He gas in healthy and diseased lungs," *Magn Reson Med,* vol. 44, pp. 174-179, 2000.

[2]   S. S. Kaushik, Z. I. Cleveland, G. P. Cofer, G. Metz, D. Beaver, J. Nouls*, et al.*, "Diffusion-weighted hyperpolarized 129Xe MRI in healthy volunteers and subjects with chronic obstructive pulmonary disease," *Magn Reson Med,* vol. 65, pp. 1154-65, Apr 2011.

[3]   S. Ajraoui, J. Parra-Robles, M. Deppe, K. Teh, S. Parnell, J. Owers-Bradley*, et al.*, "Experimental investigation of non-gaussian diffusion in hyperpolarized 3He MRI of lungs," in *Proc Int Soc Magn Reson Med*, 2009, p. 2178.

[4]   A. L. Sukstanskii and D. A. Yablonskiy, "In vivo lung morphometry with hyperpolarized 3He diffusion MRI: theoretical background," *J Magn Reson,* vol. 190, pp. 200-10, Feb 2008.

[5]   A. L. Sukstanskii and D. A. Yablonskiy, "Lung morphometry with hyperpolarized 129Xe: theoretical background," *Magn Reson Med,* vol. 67, pp. 856-66, Mar 2012.

[6]   D. A. Yablonskiy, A. L. Sukstanskii, J. C. Leawoods, D. S. Gierada, G. L. Bretthorst, S. S. Lefrak*, et al.*, "Quantitative in vivo assessment of lung microstructure at the alveolar level with hyperpolarized 3He diffusion MRI," *Proc Natl Acad Sci U S A,* vol. 99, pp. 3111-6, Mar 5 2002.

[7]   J. M. Perez-Sanchez, I. Rodriguez, and J. Ruiz-Cabello, "Random walk simulation of the MRI apparent diffusion coefficient in a geometrical model of the acinar tree," *Biophys J,* vol. 97, pp. 656-64, Jul 22 2009.

[8]   S. Fichele, M. N. Paley, N. Woodhouse, P. D. Griffiths, E. J. van Beek, and J. M. Wild, "Investigating 3He diffusion NMR in the lungs using finite difference simulations and in vivo PGSE experiments," *J Magn Reson,* vol. 167, pp. 1-11, Mar 2004.

[9]   D. S. Grebenkov, G. Guillot, and B. Sapoval, "Restricted diffusion in a model acinar labyrinth by NMR: theoretical and numerical results," *J Magn Reson,* vol. 184, pp. 143-56, Jan 2007.

[10]   D. Habib, D. Grebenkov, and G. Guillot, "Gas diffusion in a pulmonary acinus model: experiments with hyperpolarized helium-3," *Magn Reson Imaging,* vol. 26, pp. 1101-13, Oct 2008.

[11]   S. Fichele, M. N. Paley, N. Woodhouse, P. D. Griffiths, E. J. Van Beek, and J. M. Wild, "Finite-difference simulations of 3He diffusion in 3D alveolar ducts: comparison with the "cylinder model"," *Magn Reson Med,* vol. 52, pp. 917-20, Oct 2004.

[12]   R. Mair, G. Wong, D. Hoffmann, M. Hürlimann, S. Patz, L. Schwartz*, et al.*, "Probing Porous Media with Gas Diffusion NMR," *Physical Review Letters,* vol. 83, pp. 3324-3327, 1999.

[13]   G. W. Miller, M. Carl, J. F. Mata, G. D. Cates, Jr., and J. P. Mugler, 3rd, "Simulations of short-time diffusivity in lung airspaces and implications for S/V measurements using hyperpolarized-gas MRI," *IEEE Trans Med Imaging,* vol. 26, pp. 1456-63, Nov 2007.

[14]   D. D. Shanbhag, T. A. Altes, G. W. Miller, J. F. Mata, and J. Knight-Scott, "q-Space analysis of lung morphometry in vivo with hyperpolarized 3He spectroscopy," *J Magn Reson Imaging,* vol. 24, pp. 84-94, Jul 2006.

[15]   R. L. O'Halloran, J. H. Holmes, Y. C. Wu, A. Alexander, and S. B. Fain, "Helium-3 MR q-space imaging with radial acquisition and iterative highly constrained back-projection," *Magn Reson Med,* vol. 63, pp. 41-50, Jan 2010.

[16]   R. Trampel, J. H. Jensen, R. F. Lee, I. Kamenetskiy, G. McGuinness, and G. Johnson, "Diffusional kurtosis imaging in the lung using hyperpolarized 3He," *Magn Reson Med,* vol. 56, pp. 733-7, Oct 2006.

[17]   J. Parra-Robles, H. Marshall, R. Hartley, C. E. Brightling, and J. Wild, "Quantification of Lung Microstructure in Asthma Using a 3He Fractional Diffusion Approach," in *Proc. Intl. Soc. Mag. Reson. Med.*, 2014, p. 3529.

[18]   H. F. Chan, N. J. Stewart, J. Parra-Robles, G. J. Collier, and J. M. Wild, "Whole lung morphometry with 3D multiple b-value hyperpolarized gas MRI and compressed sensing," *Magn Reson Med,* vol. 77, pp. 1916-1925, May 2017.

[19]   H. F. Chan, N. J. Stewart, G. Norquay, G. J. Collier, and J. M. Wild, "3D diffusion-weighted (129) Xe MRI for whole lung morphometry," *Magn Reson Med,* vol. 79, pp. 2986-2995, Jun 2018.

[20] G. A. Paulin, A. Ouriadov, E. Lessard, K. Sheikh, D. G. McCormack, and G. Parraga, "Noninvasive quantification of alveolar morphometry in elderly never- and ex-smokers," *Physiol Rep,* vol. 3, Oct 2015.

[21] J. D. Quirk, B. A. Lutey, D. S. Gierada, J. C. Woods, R. M. Senior, S. S. Lefrak*, et al.*, "In vivo detection of acinar microstructural changes in early emphysema with (3)He lung morphometry," *Radiology,* vol. 260, pp. 866-74, Sep 2011.

[22] A. Ouriadov, A. Farag, M. Kirby, D. G. McCormack, G. Parraga, and G. E. Santyr, "Lung morphometry using hyperpolarized (129) Xe apparent diffusion coefficient anisotropy in chronic obstructive pulmonary disease," *Magn Reson Med,* vol. 70, pp. 1699-706, Dec 2013.

[23] A. Ouriadov, E. Lessard, K. Sheikh, G. Parraga, and N. Canadian Respiratory Research, "Pulmonary MRI morphometry modeling of airspace enlargement in chronic obstructive pulmonary disease and alpha-1 antitrypsin deficiency," *Magn Reson Med,* vol. 79, pp. 439-448, Jan 2018.

[24] J. D. Quirk, A. L. Sukstanskii, J. C. Woods, B. A. Lutey, M. S. Conradi, D. S. Gierada*, et al.*, "Experimental evidence of age-related adaptive changes in human acinar airways," *J Appl Physiol (1985),* vol. 120, pp. 159-65, Jan 15 2016.

[25] A. J. Hajari, D. A. Yablonskiy, A. L. Sukstanskii, J. D. Quirk, M. S. Conradi, and J. C. Woods, "Morphometric changes in the human pulmonary acinus during inflation," *J Appl Physiol (1985),* vol. 112, pp. 937-43, Mar 2012.

[26] J. P. Butler, S. H. Loring, S. Patz, A. Tsuda, D. A. Yablonskiy, and S. J. Mentzer, "Evidence for adult lung growth in humans," *N Engl J Med,* vol. 367, pp. 244-7, Jul 19 2012.

[27] E. F. Fishman, J. D. Quirk, S. C. Sweet, J. C. Woods, D. S. Gierada, M. S. Conradi*, et al.*, "What makes a good pediatric transplant lung: Insights from in vivo lung morphometry with hyperpolarized 3 He magnetic resonance imaging," *Pediatr Transplant,* Jan 24 2017.

[28] B. Haefeli-Bleuer and E. R. Weibel, "Morphometry of the human pulmonary acinus," *Anat Rec,* vol. 220, pp. 401-14, Apr 1988.

[29] D. A. Yablonskiy, A. L. Sukstanskii, J. C. Woods, D. S. Gierada, J. D. Quirk, J. C. Hogg*, et al.*, "Quantification of lung microstructure with hyperpolarized 3He diffusion MRI," *J Appl Physiol (1985),* vol. 107, pp. 1258-65, Oct 2009.

[30] A. L. Sukstanskii, M. S. Conradi, and D. A. Yablonskiy, "(3)He lung morphometry technique: accuracy analysis and pulse sequence optimization," *J Magn Reson,* vol. 207, pp. 234-41, Dec 2010.

[31] E. R. Weibel, *Morphometry of the human lung*: Springer, 1963.

[32] K. M. Bennett, K. M. Schmainda, R. T. Bennett, D. B. Rowe, H. Lu, and J. S. Hyde, "Characterization of continuously distributed cortical water diffusion rates with a stretched-exponential model," *Magn Reson Med,* vol. 50, pp. 727-34, Oct 2003.

[33] X. Liu, L. Zhou, W. Peng, H. Wang, and Y. Zhang, "Comparison of stretched-Exponential and monoexponential model diffusion-Weighted imaging in prostate cancer and normal tissues," *J Magn Reson Imaging,* vol. 42, pp. 1078-85, Oct 2015.

[34] J. Parra-Robles, S. Ajraoui, and J. M. Wild, "Modelling Non-Gaussian 3He Diffusion Signal Behaviour Using a Fractional Dynamics Approach," in *Proc Intl Soc Mag Reson Med*, 2010.

[35] M. N. Berberan-Santos, E. N. Bodunov, and B. Valeur, "Mathematical functions for the analysis of luminescence decays with underlying distributions 1. Kohlrausch decay function (stretched exponential)," *Chemical Physics,* vol. 315, pp. 171-182, 2005.

[36] G. Norquay, G. J. Collier, M. Rao, A. Maunder, O. I. Rodgers, N. J. Stewart*, et al.*, "Large-scale production of highly-polarized 129Xe," in *Proc. Intl. Soc. Mag. Reson. Med.*, 2017, p. 2140.

[37] S. B. Fain, S. R. Panth, M. D. Evans, A. L. Wentland, J. H. Holmes, F. R. Korosec*, et al.*, "Early emphysematous changes in asymptomatic smokers: detection with 3He MR imaging," *Radiology,* vol. 239, pp. 875-83, Jun 2006.

[38] A. J. Swift, J. M. Wild, S. Fichele, N. Woodhouse, S. Fleming, J. Waterhouse*, et al.*, "Emphysematous changes and normal variation in smokers and COPD patients using diffusion 3He MRI," *Eur J Radiol,* vol. 54, pp. 352-8, Jun 2005.

[39] J. Parra-Robles, H. Marshall, and J. M. Wild, "Characterization of 3He Diffusion in Lungs Using a Stretched Exponential Model," in *Proc Intl Soc Mag Reson Med*, 2013.

[40]   J. Parra-Robles, S. Ajraoui, H. Marshall, M. H. Deppe, X. Xu, and J. M. Wild, "The influence of field strength on the apparent diffusion coefficient of 3He gas in human lungs," *Magn Reson Med,* vol. 67, pp. 322-5, Feb 2012.

[41]   R. R. Mercer, M. L. Russell, and J. D. Crapo, "Alveolar septal structure in different species," *J Appl Physiol (1985),* vol. 77, pp. 1060-6, Sep 1994.

[42]   M. Ochs, J. R. Nyengaard, A. Jung, L. Knudsen, M. Voigt, T. Wahlers*, et al.*, "The number of alveoli in the human lung," *Am J Respir Crit Care Med,* vol. 169, pp. 120-4, Jan 1 2004.

[43]   L. Knudsen, E. R. Weibel, H. J. Gundersen, F. V. Weinstein, and M. Ochs, "Assessment of air space size characteristics by intercept (chord) measurement: an accurate and efficient stereological approach," *J Appl Physiol (1985),* vol. 108, pp. 412-21, Feb 2010.

[44]   J. Parra-Robles, S. Ajraoui, M. H. Deppe, S. R. Parnell, and J. M. Wild, "Experimental investigation and numerical simulation of 3He gas diffusion in simple geometries: implications for analytical models of 3He MR lung morphometry," *J Magn Reson,* vol. 204, pp. 228-38, Jun 2010.

[45]   J. Parra-Robles and J. M. Wild, "The influence of lung airways branching structure and diffusion time on measurements and models of short-range 3He gas MR diffusion," *J Magn Reson,* vol. 225, pp. 102-13, Dec 2012.
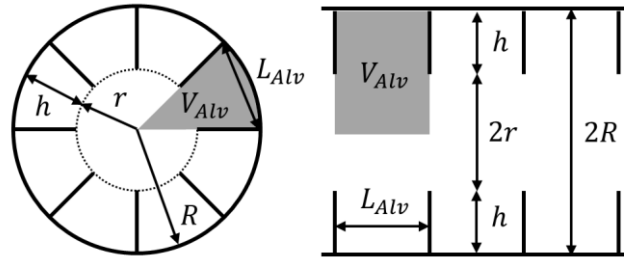
Figure 1: Cross-section of the cylinder model geometry used in this work as described in Yablonskiy et al. [29]. The acinar airway is depicted as cylinders surrounded by an alveolar sleeve, and is defined by two geometrical parameters - outer radii (R), and inner radii (r). The alveolar sleeve contains eight alveoli, therefore the length or diameter of an alveolus (L_{Alv}) is 1/8 of the cylinder chord length. The depth of the alveolar sleeve (h) is defined as R - r, and the alveolar volume (V_{Alv}) includes the volume of the alveolus and the alveolar duct.
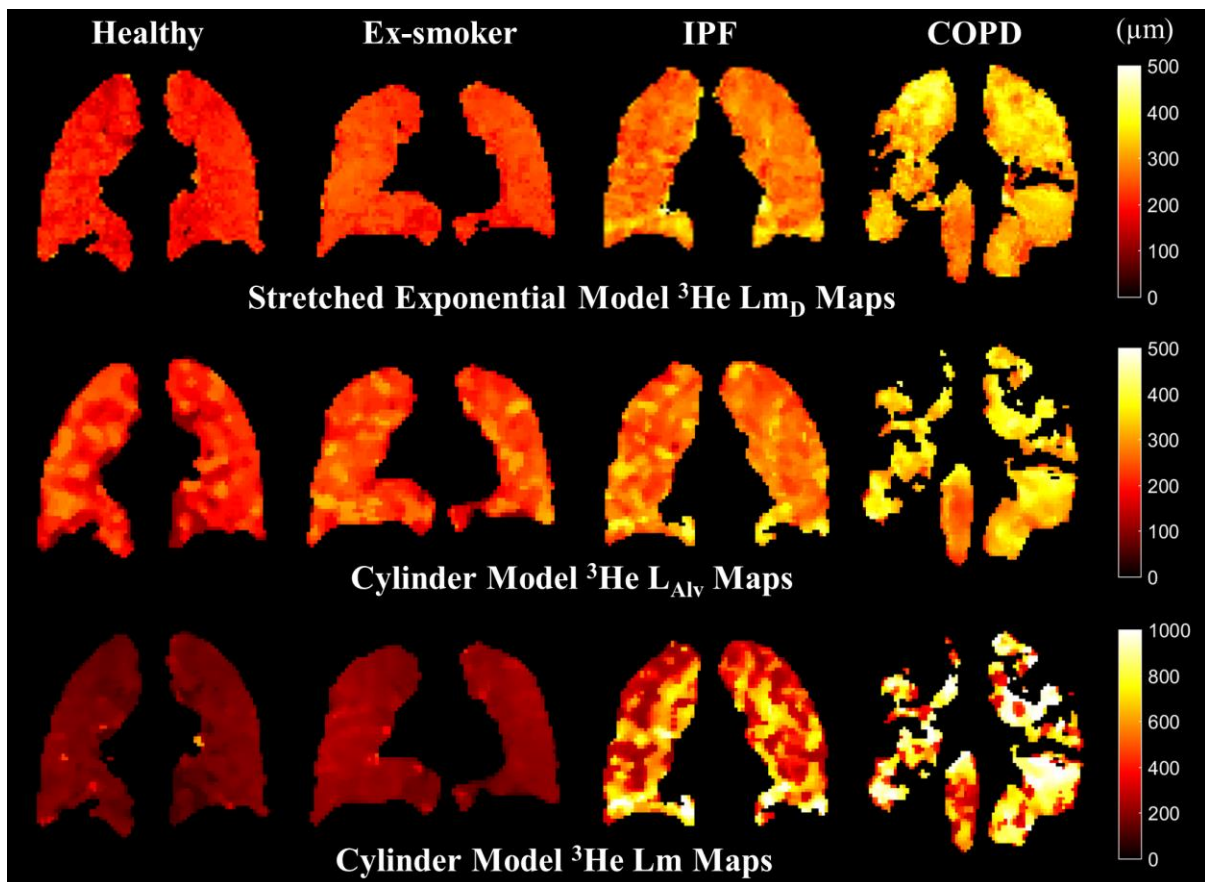
Figure 2: Representative ^{3}He maps of SEM-derived mean diffusive length scale (Lm_D), and CM-derived mean alveolar diameter (L_{Alv}) and mean chord length (Lm) for each subject group.
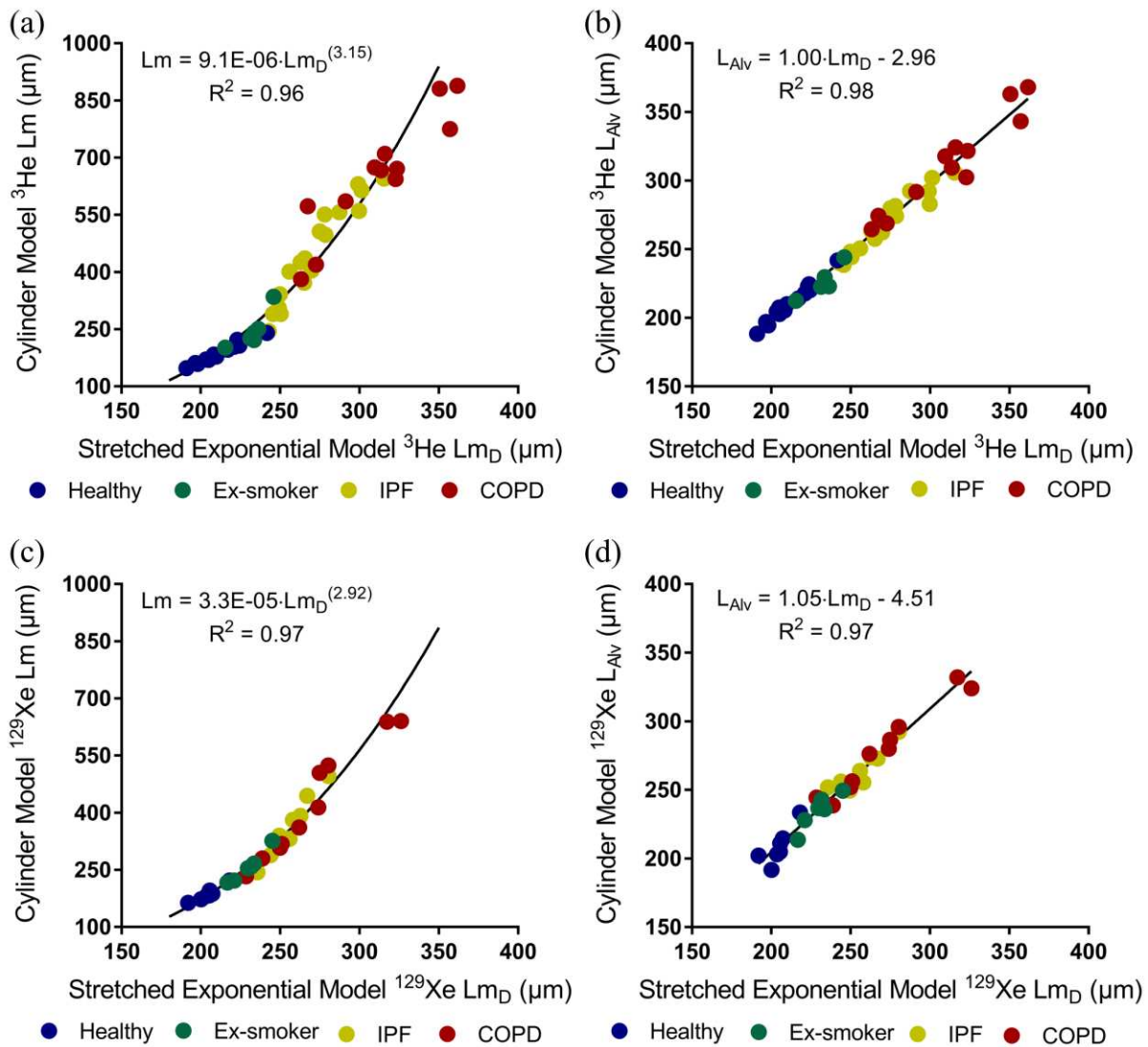
Figure 3: (a) Scatter plot of global ^{3}He Lm_D and Lm for all subjects are strongly correlated ($P<0.001$) in a power relationship. (b) Scatter plot for ^{3}He lung morphometry parameters Lm_D and L_{Alv}, which were strongly correlated ($P<0.001$) in a linear relationship and demonstrates excellent agreement between the two parameters. Equivalent scatter plots of global ^{129}Xe Lm_D and Lm (c), and ^{129}Xe Lm_D and L_{Alv} (d) for all subjects are also strongly correlated in power ($P<0.001$), and linear ($P<0.001$) relationships, respectively.
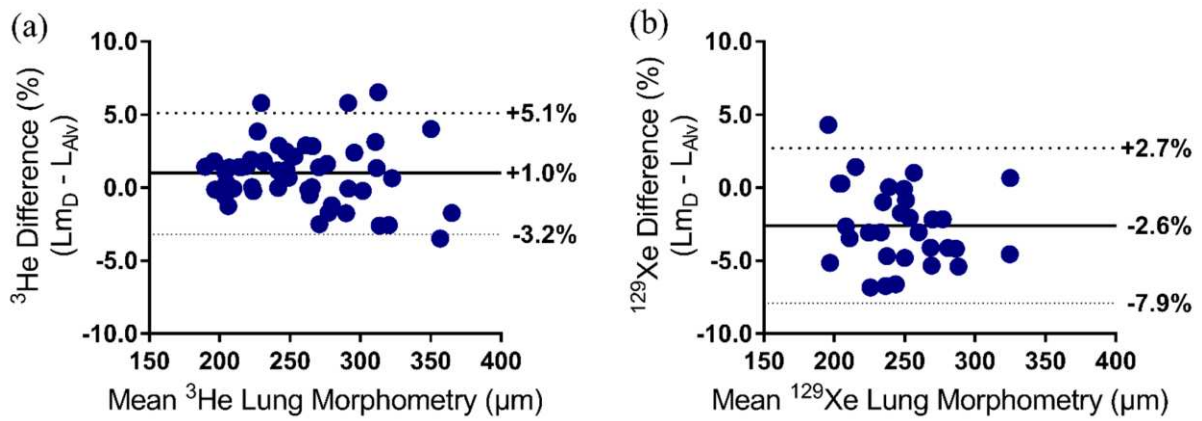
Figure 4: (a) Bland-Altman analysis of mean global ^{3}He Lm_D and L_{Alv} values. A mean of 1% towards Lm_D values was obtained with 95% of the difference between -3.2% and 5.1%. (b) The respective Bland-Altman analysis for ^{129}Xe Lm_D and L_{Alv}. A mean bias of -2.6% towards Lm_D was obtained with 95% of the difference between -7.9% and 2.7%.
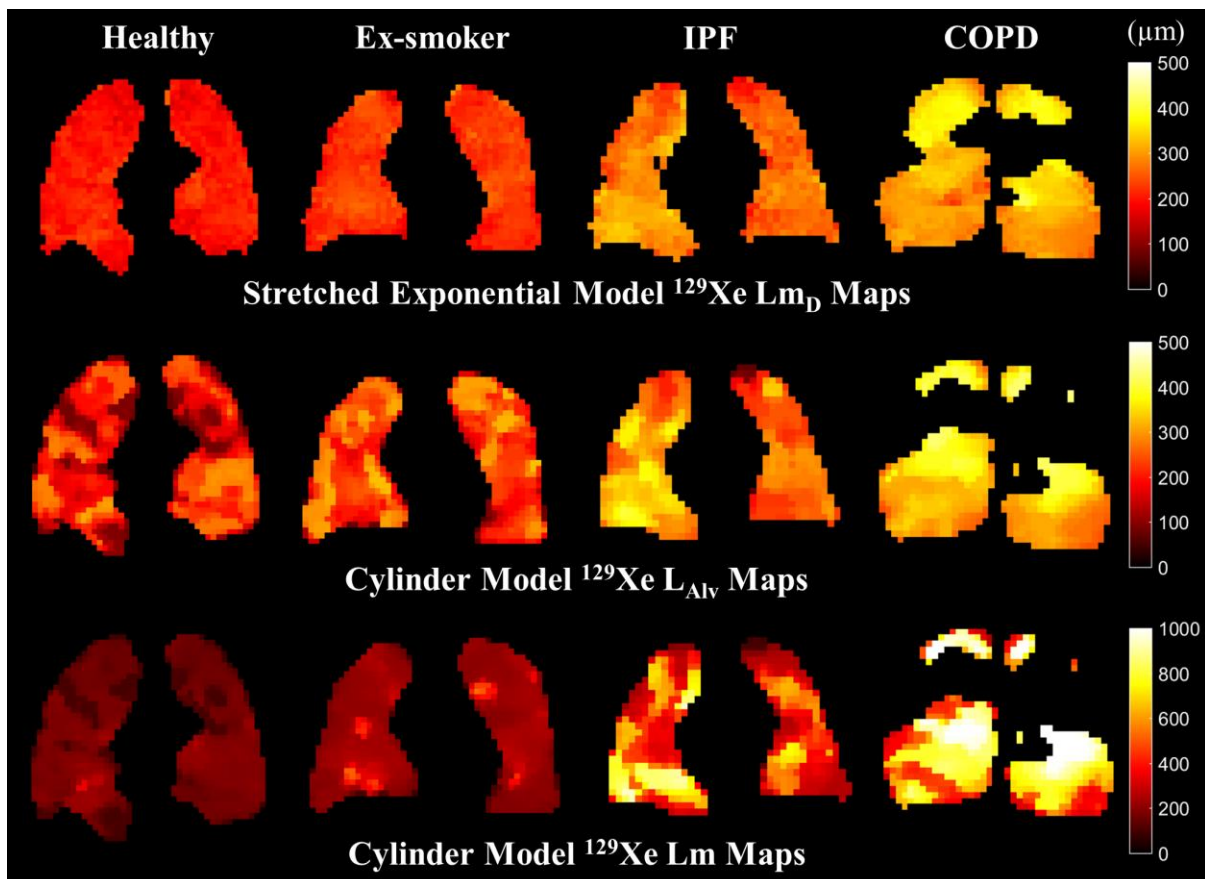
Figure 5: Representative ^{129}Xe maps of SEM-derived mean diffusive length scale (Lm_D), and CM-derived mean alveolar diameter (L_{Alv}) and mean chord length (Lm) for each subject group.
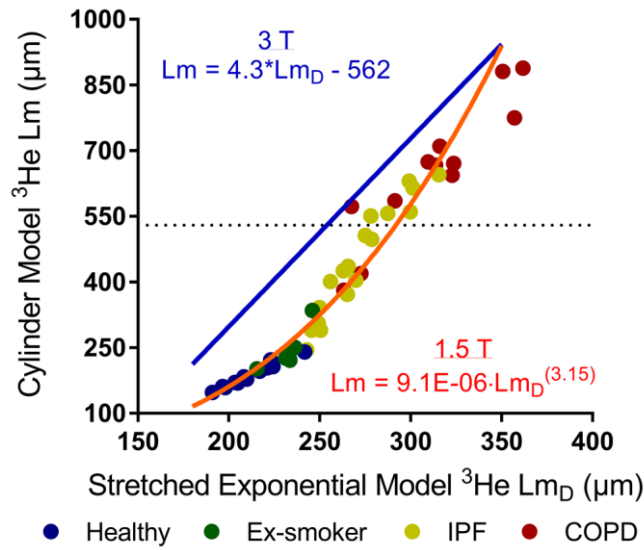
Figure 6: The linear correlation (blue line) between ^{3}He Lm_D and Lm morphometry parameters for the previous 3 T analysis of Ouriadov et al. [23] is compared against the power relationship (orange curve) observed in the comparison at 1.5 T performed here. The dotted line corresponds to the 1D free diffusion length of ^{3}He (530 µm) for the ^{3}He DW-MRI acquisition parameters.
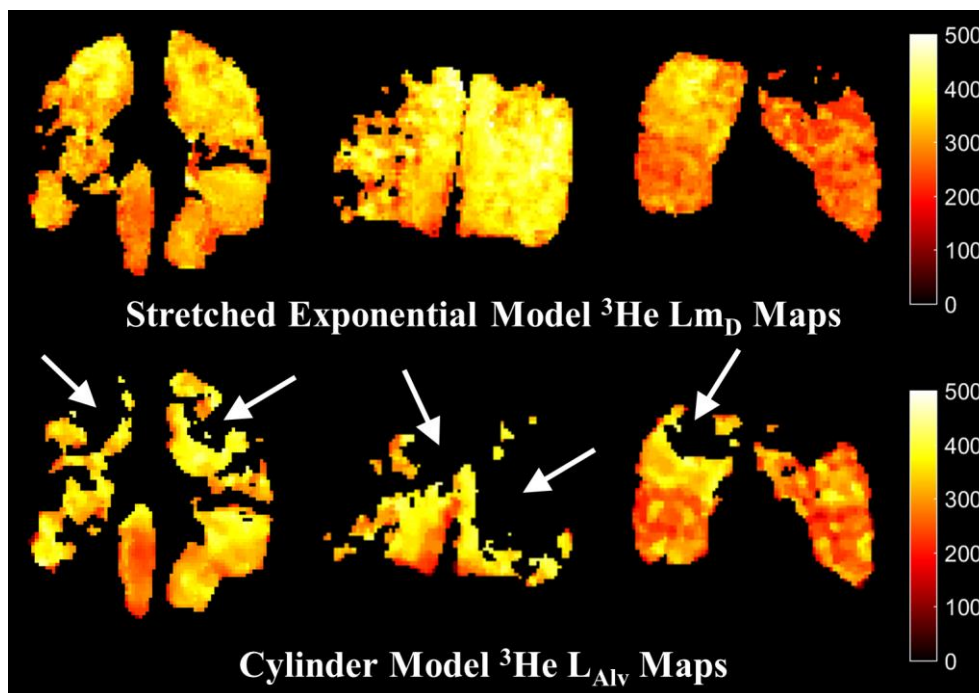

Figure 7: Representative ^{3}He Lm_D and L_{Alv} maps from three COPD patients. In the CM-derived L_{Alv} maps regions of missing voxels (white arrows) indicate areas where the physiological range of the CM is exceeded. These corresponding regions exist in the SEM-derived Lm_D maps and also coincide with regions of large Lm_D values.